

## MiCPhot: A prime-focus multicolor CCD photometer on the 85-cm Telescope \*

Ai-Ying Zhou<sup>1</sup>, Xiao-Jun Jiang<sup>1</sup>, Yan-Ping Zhang<sup>2</sup> and Jian-Yan Wei<sup>1</sup>

<sup>1</sup> National Astronomical Observatories, Chinese Academy of Sciences, Beijing 100012, China;  
[aiying@bao.ac.cn](mailto:aiying@bao.ac.cn)

<sup>2</sup> Department of Astronomy, Beijing Normal University, Beijing 100875, China

Received 2008 June 2; accepted 2008 June 18

**Abstract** We describe a new *BVRI* multicolor CCD photometric system situated at the prime focus of the 85-cm telescope at the Xinglong Station of NAOC. Atmospheric extinction effects, photometric accuracy and color calibration dependence of the system are investigated. Additional attention was paid to giving observers guidance in estimating throughput, detection limit, signal-to-noise ratio and exposure time.

**Key words:** instrumentation: photometers: CCD photometer — techniques: photometric

### 1 INSTRUCTION

With a CCD photometer, it has become possible to obtain high precision which is comparable to that of a photoelectric photometer (Walker 1990). CCD photometry shows its advantage in observing multiple and faint sources simultaneously, which is impossible using a traditional multi-channel photoelectric photometer (Nather & Mukadam 2004). As such, we have constructed the primary focus optics for the 85-cm telescope at the Xinglong Station of NAOC and installed a CCD photometer. We purchased a frame-transfer CCD camera from Princeton Instruments (PI) of Roper Scientific Inc., USA and a filter-wheel drive made by the Astronomical Consultants & Equipment Inc., USA (ACE). The standard *BVRI* filters are made by Custom Scientific, Inc. (USA).

Our scientific goal is to increase the magnitude limit and enlarge the field-of-view (FOV) with the CCD at the prime focus for high-speed time-series multiple color photometry. As of the spring of 2007, the new multicolor CCD photometer (abbreviated as MiCPhot) that consists of a PI MicroMAX:1024BFT CCD camera and a standard *BVRI* filter system started to serve astronomers. Below, we first describe the system concisely and then present some observational results in view of the system's performance. Additional materials are provided in the Appendix and are available online.

### 2 THE PRIME-FOCUS OPTICS

In place of the previous secondary mirror, a corrector with a set of lenses was constructed. The inclusion of the whole prime focus system (corrector, filter set and CCD camera) is illustrated in Figure A.1<sup>1</sup>. It is anodized black to prevent reflections in the optical system. The optical layout of the corrector is given in Figure A.2. The focusing is accomplished through an independent control box, which is connected

---

\* Supported by the National Natural Science Foundation of China.

<sup>1</sup> Note: Figures and tables not given in the text are provided in Appendix and are available online only.

**Table 1** Specifications of PI MicroMAX:1024BFT Camera

Attribute	Specifications
CCD image sensor CCD format	Marconi CCD47-20 (BFT): back-illuminated, frame-transfer CCD 1024 × 1024 imaging pixels; 13.0 × 13.0- $\mu\text{m}$ pixels size; 13.3 × 13.3-mm imaging area (optically centered)
On-chip storage Grade	1024 × 1024, frame transfer operation Grade 1: $\leq 100$ dark defects, $\leq 5$ traps, $\leq 2$ column defects (based on CCD manufacturer's cosmetic blemish definitions)
Linear full well	(1) single pixel: Typical: $> 60,000 e^-$ (factory-tested value: $68,000 e^-$ ) (2) $2 \times 2$ binned pixel: Typical: $> 200,000 e^-$
Readout noise	(1) 2-MHz: $11.5 e^-$ (typical) (2) 1-MHz: $8$ (typical) $-10 e^-$ rms (maximum) (3) 100-kHz: $4$ (typical) $-5 e^-$ rms (maximum)
Readout bits/speed	16 bits @ 50, 100, 200, 500, 1000, 2000-kHz digitization
Frame readout time	1.1 seconds for full frame @ 1-MHz with no binning, see Table 2
Frame transfer time	1.24 ms = $310 \mu\text{s} \times 4$
Gain	$2 e^-/\text{ADU}$ at medium setting
Spectral range	typical: 350–1000 nm
Dark noise	$< 10 e^-/\text{pixel}/\text{sec}$ (factory-tested value: 7.8) @ $-40^\circ\text{C}$
Nonlinearity	$< 2\%$
Quantum efficiency	30% at 3500 $\text{\AA}$ , 80% in 4500–6500 $\text{\AA}$ , 40% at 9000 $\text{\AA}$ , see Fig. A.3
Chip temperature	$-45^\circ\text{C}$
Operating environment	$0^\circ - 30^\circ\text{C}$ ambient, 0%–50% relative humidity, non-condensing

to the same computer that controls the CCD camera and filterwheel. The prime focus optics have been designed in a compact space within 100 mm (excluding the camera) along the optical axis to allow more space for star light, while the original secondary mirror occupied some 400-mm of space; The corrector is position adjustable. Its effective working wavelength range is 380–900 nm with the possibility of color extinction in each of the *BVRI* bands. The optical system finally has a measured effective FOV of  $16'.5 \times 16'.5$  at a focal ratio of 3.27 ( $f = 2780$  mm) with a scale of 0.96 arcsec per pixel for the 1024 CCD. Focusing is driven by a step motor and is adjustable in a range of  $\pm 10$  mm in steps of 0.001 mm by moving the CCD camera relative to the fixed corrector. Focusing is controlled via stand-alone computer software. In addition, it has the following features: (1) coefficients of vignetting had been designed to be within 0.076, 0.062, 0.048 and 0.029 arcsec for the full, 0.85, 0.7 and 0.5 FOV, respectively; (2) useable for both 1024 (13- $\mu\text{m}$ ) and 2048 (12- $\mu\text{m}$ ) CCD cameras with the corrector's aperture size of 80 mm; (3) elimination of locally scattered light to ensure variations in the flat-field images are within a few percent.

### 3 THE MULTI-COLOR CCD PHOTOMETER SYSTEM

#### 3.1 The CCD Camera

The PI MicroMAX:1024BFT camera (with a rectangular head) is a high-resolution device that combines the sensitivity of back-illuminated technology with the speed of frame-transfer readout. The cooling system allows the MicroMAX camera to typically maintain a temperature of  $-45^\circ\text{C}$ . The standard MicroMAX controller (model ST-133B) enables both high-speed and high-precision readout capabilities. It can collect 16-bit images at a readout rate of up to 2 million pixels per second (i.e. 2 MHz) in the high-speed mode or at 50 thousand pixels per second (50 kHz) in the optional precision mode. There are six readout rates to select with the software control. The specifications of the CCD camera are provided in Table 1, while Table A.1 lists additional features and benefits of the camera. The thin back-illuminated CCD array has a broad-band anti-reflection coating. This gives  $>80\%$  peak quantum efficiency in the range 450–650 nm. Detailed wavelength response is shown in Figure A.3. Image display orientation on the computer monitor is north up and east to the left.

**Table 2** Readout time ( $t_r$ , in seconds) and readout noise ( $\sigma_{\text{ron}}$  in units  $e^-$  rms) at gain of  $1.17 e^-/\text{ADU}$ . A subframe of  $400 \times 400$  is only given for 1 MHz. Two rates at 50 and 200 kHz and less used modes are not tested.

Read Rates		Binning			
		$1 \times 1$	$2 \times 2$	$3 \times 3$	$4 \times 4$
2 MHz	$t_r$	0.50	—	—	—
	$\sigma_{\text{ron}}$	11.51	—	—	—
1 MHz	$t_r$	1.09	0.417	0.266	0.178
	FPS	0.91	2.40	3.76	5.60
	$\sigma_{\text{ron}}$	8.6	8.46	9.29	9.89
500 kHz	$t_r$	2.00	—	—	—
	$\sigma_{\text{ron}}$	6.5	—	—	—
100 kHz	$t_r$	11.18	3.38	2.38	1.43
	$\sigma_{\text{ron}}$	4.93	5.74	8.01	9.28
1 MHz		Region $400 \times 400$			
	$t_r$	0.357	0.178	—	0.105
	FPS	2.8	5.6	—	9.5

Analog gain control can be used to change the number of electrons required to generate an Analog-to-Digital Unit (ADU, also known as a count). Therefore, a low gain is commonly used for bright objects, while high gain is for faint objects. A gain value is expressed in units of electrons per count. There is a gain switch on the camera. It has three settings: high, medium and low, which correspond to a gain of about 1.05, 1.94 and  $3.86 e^-/\text{ADU}$ , respectively. In most instances, the medium setting should generally give an overall noise of  $\sim 1$  count or  $\sim 9.23 e^-$  rms. The observer must select the gain setting so that at the desired exposure time, the stars of interest have counts between 8000 and 35 000, placing the observations in the linear regime of the CCD while optimally using the dynamic range (refer to Fig. C.4). The amplifier gain selection can also be made via the control software. When software-selection of gain is available, the software selection will override any hardware setting. However, when the ST-133 model controller is used (i.e. our case) the hardware switch is deactivated. Our practical test shows that the gain is automatically set to high (measured  $\sim 1.17 e^-/\text{ADU}$ ) when using the ST-133B controller and MaxIm DL Version 4.11 software — this software does not provide alternative gain options.

In addition, the CCD software provides binning and subframe operations. The former is the process of adding the data from adjacent pixels together to form a single pixel (sometimes called a super-pixel). We have measured readout noises and actual readout times for different read rates. Table 2 gives the readout times in different configurations of pixel binning and subframe, in normal readout mode. Frame readout rates (in frames per second – FPS) correspond to the reciprocal readout times.

In Figures 1 and 2, we provide an on-axis and off-axis point spread function (PSF) of the system as an indication of imaging quality. These were measured with the real images of a field centered on the standard star 98 670 taken during moderate weather conditions.

### 3.2 Filter System

The filter system consists of filters, filterwheel and filter box. Our standard Johnson-Cousin-Bessel set *BVRI* filters are manufactured by the Custom Scientific, Inc. (USA) according to the Bessell (1990) formula. They are integrated with a filter wheel of model ACE SFW-32-8-S, which is placed in an ACE SmartFilter™ for single filter box. There are eight holes in the wheel to accommodate eight 32-mm square filters. The filter box is controlled using an RS232 serial port independently via the hyper-terminal under Microsoft Windows. However, the filter box or filter system is also controllable using MaxIm DL software. In addition to the *BVRI* filters, a ‘clear’ piece for unfiltered observations is also supplied. The transmission curves of the *BVRI* filters are given in Figure A.4. The central wavelengths and passbands in nanometers are (440, 100), (550, 90), (630, 120) and (790, 300) for *BVRI* respectively. As the optical correctors’ effective working wavelength is limited to 380–900 nm,

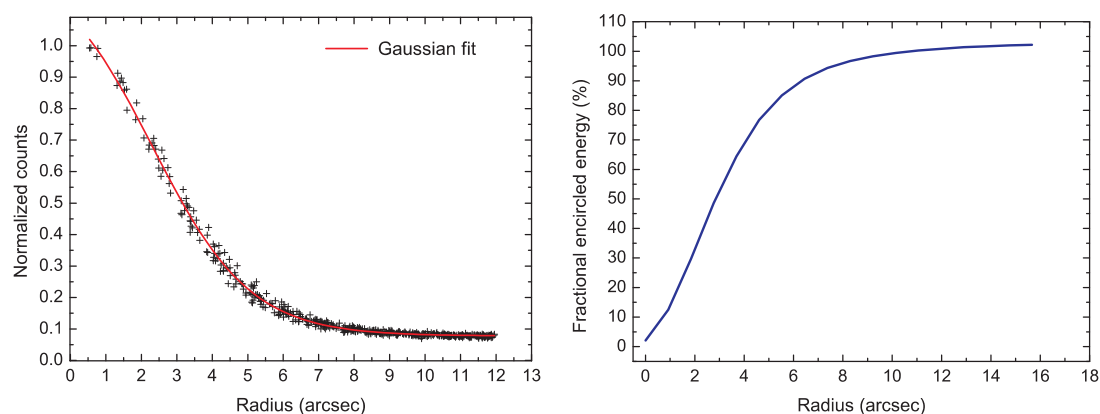


**Fig. 1** On-axis radial count distribution (left) and fractional encircled energy as a function of angular radius.

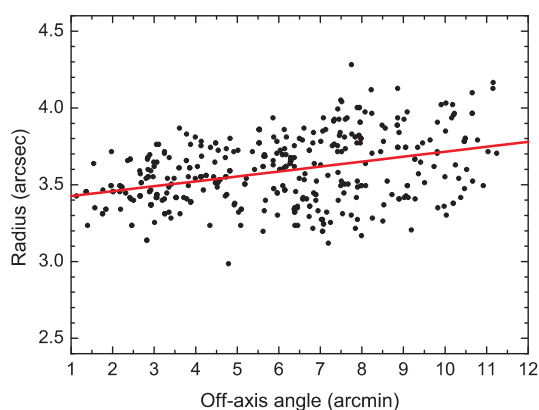


**Fig. 2** Gaussian profile radii of 406 stars measured as a function of off-axis angle. The radii refer to the values at which 90% of the total energy is encircled on the off-axis angles.

light in the  $U$  band (though we also have the  $U$  filter) is basically cutoff and then cannot be used in photometry. The wheel uses a positive mechanical detent locking system to ensure filters return to the same position for perfect flat fields. We measured the average time needed to rotate the filter wheel from a filter to its neighbor, and the value is about 2.57 s.

### 3.3 Camera Control Computer and Timing

The CCD camera connects to an ST-133B controller (A/D converter, mounted near the end of the telescope's tube) via an analog cable. An interface PCI card housed in the camera control computer connects to the controller via a 30 meter digital high-speed communication cable. Also inserted into the computer is the interface card which controls the focusing device. The personal computer (PC) also needs an ethernet card to connect to the Internet so that the Network Time Protocol (NTP) software can interface with the system clock. At the beginning of an observation and whenever needed during the night, an observer needs to run a standalone focusing-control program to adjust the focus.

A time-series photometer must know precisely when an exposure is started, and precisely how long it takes. Accurate timing is crucial for the frame-transfer operation and high-speed photometry.

**Table 3** Atmospheric Extinction Coefficients at Xinglong

Year	$k'_B$	$k'_V$	$k'_R$	$k'_I$
2008	$0.330 \pm 0.007$	$0.242 \pm 0.005$	$0.195 \pm 0.004$	$0.066 \pm 0.003$
1995	0.35	0.20	0.18	0.16
1989	0.31	0.22	0.14	0.10

However, the data-acquisition software gets time from the PC clock, which always has a drift compared to the standard clock. Therefore, we currently use NTP software to frequently correct the PC clock. The software (NETTIME) obtains timing information over the Internet by periodically (e.g. every six minutes) contacting several nearby time servers and adjusting the PC system clock accordingly. It allows for internet time delays as well as it can and averages the best readings it finds to keep the PC system clock in proper synchronization. We find a common timing precision within a few milliseconds.

### 3.4 Online Image Reduction and Real-Time Light Curves

We have developed an online image reduction program for the CCD photometer in order to monitor the variability of the target and also weather changes. It displays the real-time light curves of the target, one or two comparison stars, sky background and the difference between the target and the comparison stars. Besides doing online photometry, the program also calculates signal-to-noise ratios (SNR) and the uncertainty of the target in each image. For calculations, refer to Appendix D. The SNR values provide a guide for refining an observing night in order to optimize telescope time and ensure data quality.

## 4 CAMERA PERFORMANCE AND SYSTEM CALIBRATION

In order to provide observers with a general knowledge of the atmospheric extinction and color transformations of the new multi-color CCD system, we have collected the data of some photometric standard stars. We performed aperture photometry based on the calibrated images. The procedures of data reduction, which include bias subtraction, dark reduction, flat-field correction and magnitude extraction are outlined in Zhou et al. (2006). The data are described and analyzed in the followings sections. The results are presented for the purpose of calibration and signal-to-noise reference. Miscellaneous tests conducted to evaluate the CCD photometer's performance are given in Appendix.

### 4.1 Atmospheric Extinction

As an estimate of extinction effects through atmospheric transmission and the response of the telescope's optics, filters and detector, we observed the open cluster M67 in the *BVR* bands with one field especially around the known  $\delta$  Scuti star EX Cnc on 2007 November 30, as well as the field centered on GSC 0880–0055 in *BVI* on 2008 February 14. Data were acquired on a Moonless photometric night. We took a complex approach by using not only the standard stars but also those known to be non-variables. The assembly photometry (arithmetic mean) of at least three to seven stars in each field was used to study the extinction dependence on airmass and colors. We just took the main extinction into consideration while the second-order extinction is ignored. Figure 3 reports the results, which represent a common winter condition – dome seeing of about 3.0 arcsec. The extinction coefficients are given in Table 3 and compared with two sets of values for the site given by Shi et al. (1998).

### 4.2 *BVRI* Throughputs and Color Transformations

With the new multi-color CCD photometer, we have observed a set of *UBVRI* photometric standard stars near the celestial equator (Landolt 1992) for system calibration. A Landolt equatorial field centered on the standard star 98 670 was observed on a Moonless photometric night when it was close to zenith. The field was exposed twice in each of the *BVRI* bands with identical integration times for each filter. Fortunately, there are more than twenty standard stars in the frame. We had combined the two

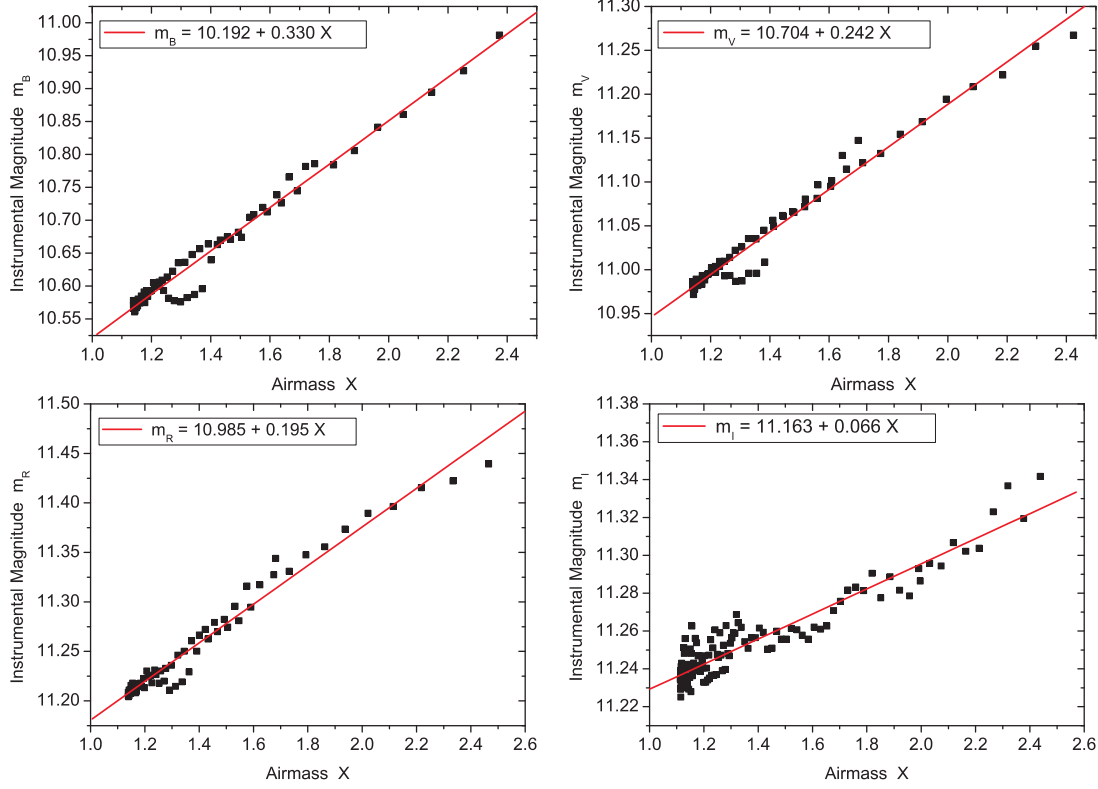


**Fig. 3** Bouguer extinction lines in  $B$ ,  $V$ ,  $R$ ,  $I$  bands, see Table 3.

series of  $BVRI$  frames by averaging them. The observed equatorial photometric standard stars were first measured with the data-taking software MaxIm DL for observers' direct reference, then they have been calibrated, photometrically measured and analyzed to transform the instrumental magnitudes to a standard system. Investigations on throughputs and SNR are given in Appendix.

Concerning the CCD photometer system calibration, the instrumental magnitudes are defined as

$$\text{mag} \equiv 23.2 - 2.5 \log(\text{flux}/\text{exptime})$$

so that the values are close to those standard magnitudes, where  $\text{flux}/\text{exptime}$  refers to encircled counts per second. The extracted individual instrumental magnitudes of 22 selected standard stars (ten of them are listed in Table D.1) were converted to their exoatmospheric values using the extinction coefficients. Finally, we transformed our instrumental magnitudes into the standard system. The results are plotted in Figures 4 and 5, where the least-squares fittings which represent the color transformations are presented in Equations (1) to (5) along with fitting errors. The lower-case letters represent the instrumental magnitudes (corrected for exposure time and photometry aperture), while the upper-case symbols indicate magnitudes in the standard system. 'X' stands for airmass and the subscript '0' in Figure 4 denotes exoatmospheric magnitudes.

$$B - V = -0.172 \pm 0.014 + (1.202 \pm 0.014)(b - v) - (0.106 \pm 0.009)X, \quad \sigma = 0.030 \quad (1)$$

$$V - R = 0.255 \pm 0.008 + (0.977 \pm 0.017)(v - r) - (0.046 \pm 0.005)X, \quad \sigma = 0.027 \quad (2)$$

$$R - I = 0.456 \pm 0.006 + (0.818 \pm 0.018)(r - i) - (0.102 \pm 0.005)X, \quad \sigma = 0.028 \quad (3)$$

$$V - I = 0.741 \pm 0.009 + (0.898 \pm 0.012)(v - i) - (0.154 \pm 0.007)X, \quad \sigma = 0.038 \quad (4)$$

$$V = v + 0.058 \pm 0.014 - (0.111 \pm 0.013)(B - V) - (0.330 \pm 0.007)X, \quad \sigma = 0.035 \quad (5)$$

Providing  $V$  and the color indices  $(B - V)$ ,  $(V - R)$ ,  $(V - I)$ , individual magnitudes in  $BRI$  can be found by  $B = V + (B - V)$ ,  $R = (R - I) - (V - I) + V$  and  $I = V - (V - I)$ . Observers doing absolute photometry are encouraged to improve these transformations in their research efforts by taking additional observations and further measurements, such as those given by Cousins & Caldwell (2001).

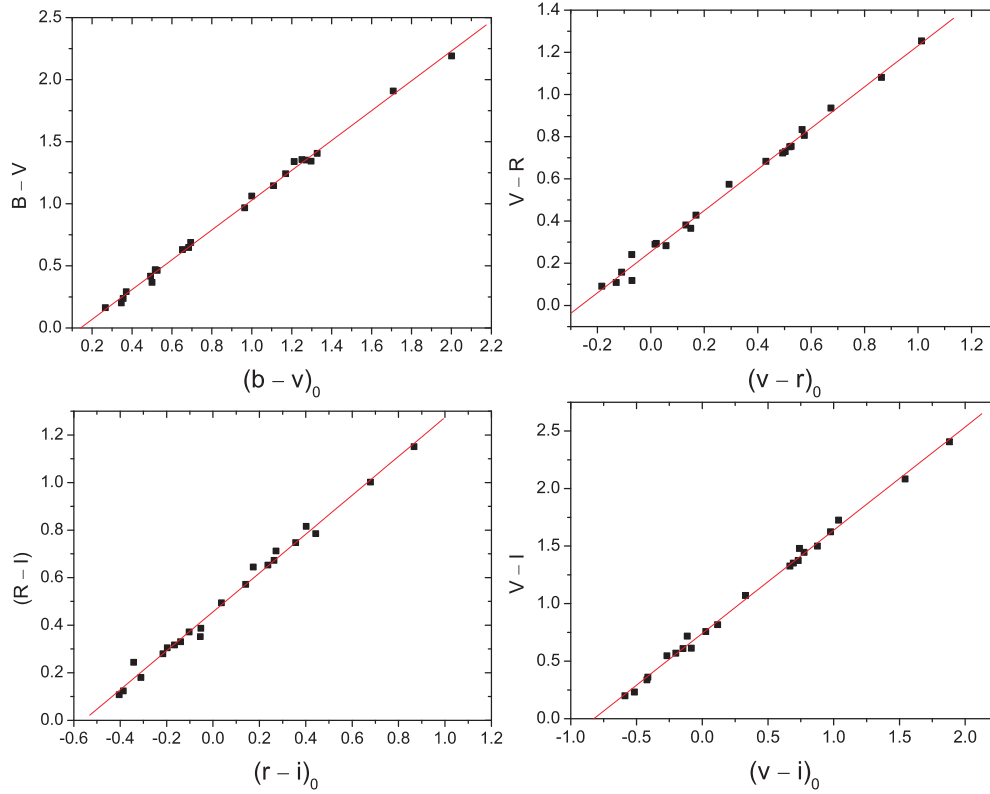


**Fig. 4** Color transformations for  $(B - V)$ ,  $(V - R)$ ,  $(R - I)$  and  $(V - I)$ , see Eqs. (1)–(4).

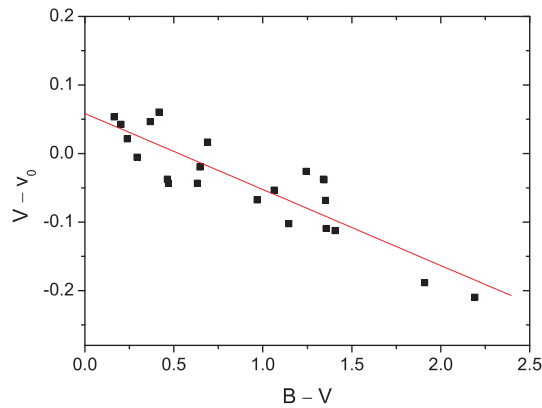


**Fig. 5** Color transformation —  $(V - v_0)$  vs.  $(B - V)$ , see Eq. (7).

### 4.3 Photometry Accuracy

We used independent measurements on two frames of a field centered on the standard star 98 670 in order to estimate the actual photometric precision. Figure 6 shows the results, where the precision is better than 0.02 mag in 12–15 mag in the  $V$  band during a 20-s exposure. Larger scatter on stars fainter than 15 mag is due to short exposure. For absolute photometry, the precision will also be constrained by the calibration equations that would generally have the error bars of 0.035, 0.035, 0.038 and 0.038 mag for  $BVRI$ , respectively. Careful exposure and better weather conditions would improve the photometric accuracy. In Figure D.4, we present a set of non-variable stars' measurements from the V577 Oph field for a general evaluation of differential photometry's data scatter. The standard deviations for each set (from top to bottom) are  $\sigma = 0.0036, 0.0047, 0.0049, 0.0056$  mag.

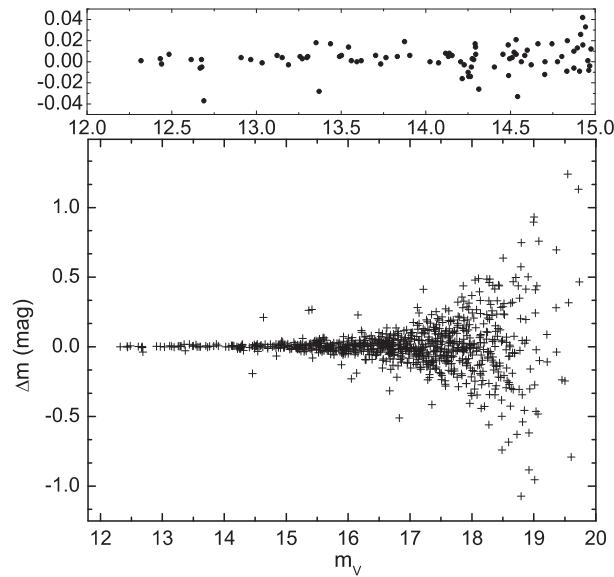


**Fig. 6** Scatter of two sets of independent measurements of 858 stars in the field centered on the standard star 98–670 with a 20-s exposure in the  $V$  band. Top panel shows a zoom-in at 12–15 mag.

## 5 ENDING REMARKS

With MiCPhot, the new prime-focus multi-color CCD photometer, observers can do  $BVRI$  sequential photometry on a fast-readout mode with short readout time down to 1 s or less if working in frame transfer mode. An online image reduction and light-curve display program has been developed to monitor the variability of the target and control data quality during observations. The current work has paid attention to exploring exposure throughputs, atmospheric extinction effects and color transformations of the system for ordinary observing conditions.

As for a dedicated precise multi-color photometry system, an automatic guiding system is expected to be made available. A dome flat field system is indispensable as a substitute for taking the twilight or dawn sky flats in some case. As a substitute, another precision timekeeping system (better than 1 ms) based on a local Global Positioning Signal (GPS) clock is under consideration. GPS and NTP will compensate each other for assuring data quality in the case of either no Internet connection or local GPS time signals being unavailable. A further consideration is to purchase an alternative set of Strömgren intermediate  $uvby\beta$  filters to provide observers another multi-color photometry system.

**Acknowledgements** The 85-cm telescope is sponsored by both the Xinglong Station of National Astronomical Observatories of Chinese Academy of Sciences (CAS) and the Department of Astronomy, Beijing Normal University under a cooperative agreement. This work was funded by the National Natural Science Foundation of China (NSFC) and CAS joint fund on astronomy under project No.10778624.

**Appendix A: OPTICS AND CAMERA**

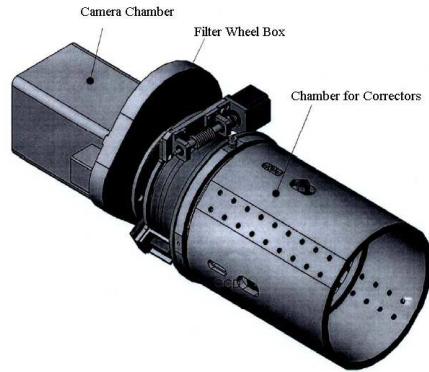


**Fig. A.1** Configuration of the prime focus system. The enclosure is anodized black.

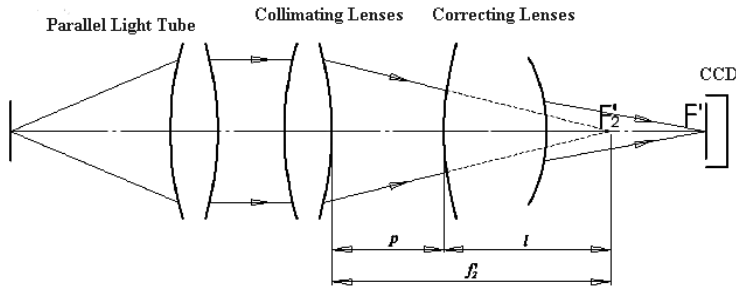


**Fig. A.2** Optical layout of the corrector of the 85-cm telescope's prime focus system.

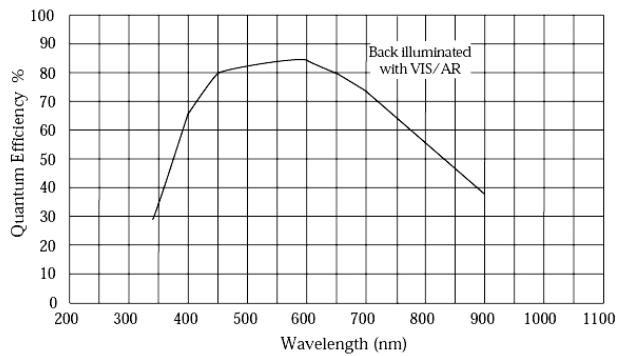


**Fig. A.3** Quantum Efficiency of the PI MicroMAX:1024BFT CCD.

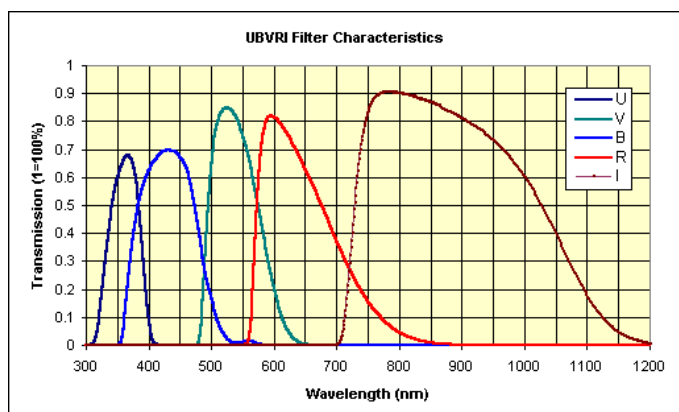


**Fig. A.4** Transmission curves of *UBVR* filters ranged from left to right are *U*, *B*, *V*, *R*, *I*, respectively.

**Table A.1** Features and Benefits of PI MicroMAX: 1024BFT Camera

Features	Benefits
1024 × 1024 imaging array	Highest resolution available in a back-illuminated format
Back-illuminated CCD	Highest sensitivity throughout the visible spectrum
Frame-transfer readout	Fast image readout (normal mode) and shutterless operation (frame-transfer mode): shutter compensation time: 200 ns
Low-noise readout	Able to measure smaller signals
Flexible binning and readout	Increases light sensitivity while increasing the frame rate
16-bit digitization	Quantifies both bright and dim signals in the same image
Cooling	Thermoelectric & fan air exhaust allows stable working around $-40^{\circ}\text{C}$ and long integration times for higher sensitivity
C-mount	Easily attaches to standard lenses or optical equipment
Shutter	25-mm internal shutter: Electronic: 6 ms; small: 8 ms
PCI interface	Works with PC or Macintosh
Video output	Compatible with standard video equipment

## Appendix B: FRAME TRANSFER OPERATION

In most cases, we operate the CCD in the standard timing mode of full-frame readout (sized  $1024 \times 1024$ ) with shutter control. Besides the normal mode, the MicroMAX:1024BFT CCD fully supports frame transfer readout. In frame transfer operation (sized  $1024 \times 2048$ ), half of the CCD array is used for sensing light and it is exposed continuously, raising the exposure duty cycle to nearly 100%. The other half of the CCD is shielded to prevent exposure for storage and readout, and it is here that the images are stored until they can be readout.

Figure B.1 shows the readout of a masked version of a schematic  $4 \times 6$  CCD array. The shading represents the masked area (masking is on the array). Only the exposed region collects charge. At the end of the exposure, the charge is quickly shifted into the masked region. Since the shifting is accomplished in a short time, i.e. a few milliseconds, the incident light causes only minimal “smearing” of the image. While the exposed region continues to collect data, the masked region is readout and digitized. The percentage of smearing can be determined by dividing the time needed to shift all rows from the imaging area by the exposure time.

Here we illustrate exposure and readout modes under the frame-transfer operation. There are two modes: Non-Overlap and Overlap. The Non-Overlap mode allows one to expose the array for the ex-

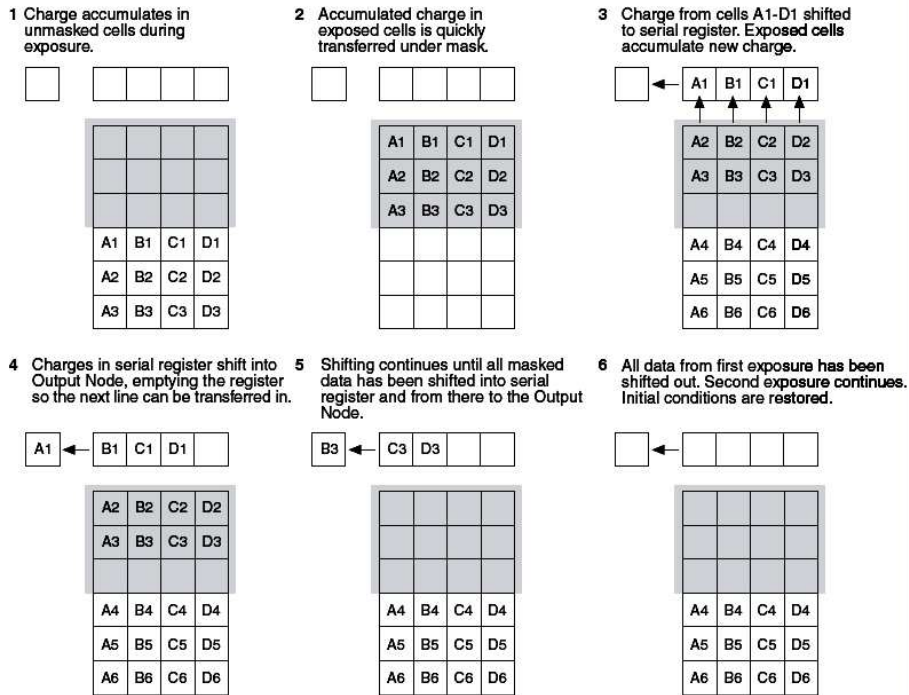


Fig. B.1 Frame transfer readout – illustration for 4x6 CCD.

posure time specified in the software and is similar in performance to a normal, full-frame device. For a 10 ms exposure, assuming a 34.8 ms readout time, the total time for 3 frames is  $3 \times 10 + 3 \times 34.8 = 134.4$  ms, which is equivalent to a frame rate of 22.3 fps. The operational sequence is (1) clearing the CCD array; (2) exposing for the specified exposure time; (3) shifting the image from the sensor area to the frame-transfer area; (4) reading out the CCD. The Overlap mode means simultaneous exposure and readout. Once a frame is exposed and transferred into the storage area, the next exposure immediately starts and continues until the previous frame is read out or until the exposure time is finished, whichever is longer. Therefore, the minimum effective exposure time is the readout time. For example, for a 10 ms exposure, 34.8 ms readout, the total time to acquire 3 frames is  $10 + 3 \times 34.8 = 114.4$  ms. If the exposure time is set to 50 ms with the readout time remaining at 34.8 ms, the time taken to acquire 3 frames will be  $3 \times 50 + 34.8 = 184.8$  ms (equivalent to a frame rate of 16.2 fps).

## Appendix C: CAMERA EXAMINATIONS

### C.1. Bias Level and Dark Current Characterization

We tested the bias level at the chip temperature of  $-45^\circ\text{C}$ , winter ambient temperature of  $-5^\circ\text{C}$  and 100 kHz read rate. The bias distribution of about  $90 \pm 20$  ADU  $\text{pixel}^{-1}$  along a central column and a line is shown in Figure C.1.

We have measured the dark counts as a function of the exposure time for  $1 \times 1$  (unbinned) and  $2 \times 2$  binning. At each integration, in which times ranged from 10 to 900 s, three dark frames were obtained. Readout rate was set to 100 kHz and gain at medium. The CCD was working at a cooling temperature of  $-50^\circ\text{C}$  and the ambient temperature was around  $-8^\circ\text{C}$ . The unbinned pixel accumulates dark counts of about  $1.8$  ADU  $\text{pixel}^{-1} \text{s}^{-1}$  while with  $2 \times 2$  binning we got  $7.4$  ADU  $\text{pixel}^{-1} \text{s}^{-1}$ , a value which falls in the expectation of four times as much as an unbinned pixel. Figure C.2 shows the results, where the fitted lines are described as:  $(70.3 \pm 1.1) + (1.847 \pm 0.003)\Delta t$  with fitting standard deviation  $\sigma = 4.75$

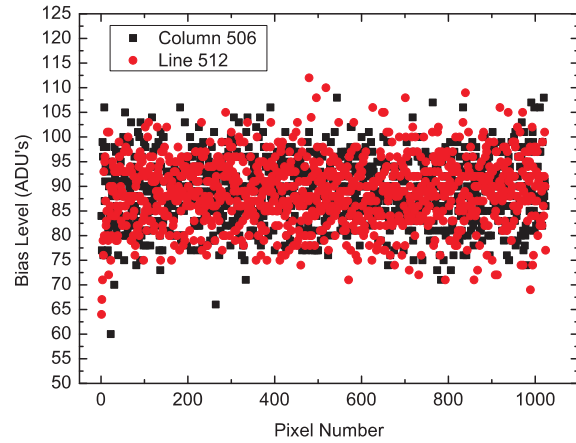


**Fig. C.1** Bias level distribution at  $-45^\circ\text{C}$  and 100 kHz read rate in the central chip.

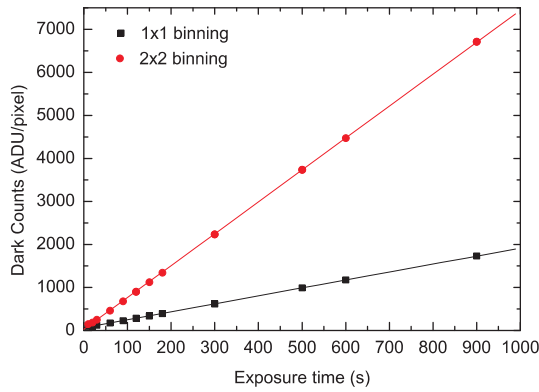


**Fig. C.2** Dark counts shown as a function of exposure time for the  $1\times 1$  and  $2\times 2$  binning settings.

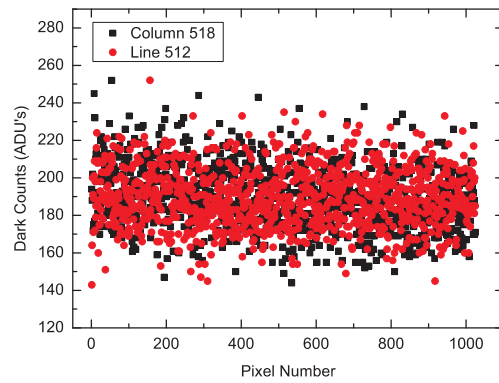


**Fig. C.3** Dark current distribution at  $-45^\circ\text{C}$ , 100-kHz read rate and 30-s exposure in central chip.

and  $(26.6 \pm 7.4) + (7.41 \pm 0.01)\Delta t$  with  $\sigma=19.8$  for  $1\times 1$  and  $2\times 2$  binning, respectively. In general, an observer can expect a dark current of  $n^2$  times  $1.85\text{ ADU pixel}^{-1}\text{ s}^{-1}$  for  $n\times n$  binning at  $-45^\circ\text{C}$ . Our data show that this is true when integration times are longer than 120 s. When dark counts are less than 60 s, they do not increase following this rule but are actually lower — less than 2 times  $1\times 1$  values for  $2\times 2$  binning when exposures are shorter than 30 s. The measured values are much better than the factory ones (see Table 1). A dark distribution of about  $6\text{ ADU pixel}^{-1}\text{ s}^{-1}$  taken at  $\Delta t = 30\text{ s}$ ,  $-45^\circ\text{C}$  and 100 kHz read rate along a central column and line is shown in Figure C.3.

## C.2. Linearity and Gain

We want to test whether our CCD is linear, i.e. whether the level we read out (when the bias has been subtracted), is proportional to the integration time. Our goal is to acquire photometry at the milli-magnitude level. To attain this precision, it is important that no artifacts, such as slow shutter speed or chip non-linearity, enter the data reduction. To check for these effects, we obtained images of the dome during a perfectly clear day with the Sun high in the sky (attempted constant light source), with the dome shutter slightly opened and pointed in the opposite direction of where the telescope points (to a reasonably

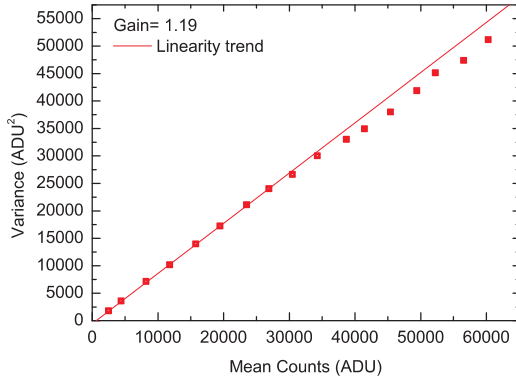


**Fig. C.4** Photon transfer curve shows the CCD's linearity up to 35 000 counts. The measurements indicate a gain of  $1.19 e^-/\text{ADU}$  and readout noise of  $8.6 e^-$  rms.

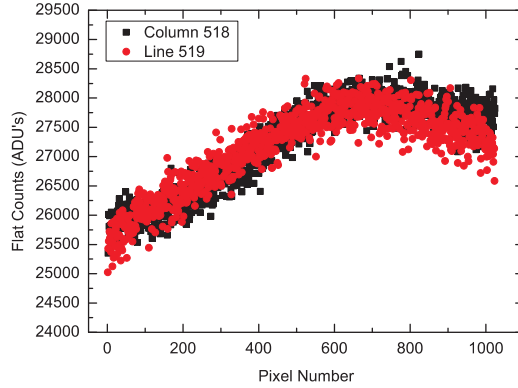


**Fig. C.5** Flat distribution of the central chip.

blank portion of the dome interior). Approximately 30 s integrations were chosen so that the intensity of the illumination reaches saturation of the CCD chip. We acquired two sets of daylight flats with the same exposure times in a sequence with random order (in steps of 1 or 0.5 second) spanning the full range of the CCD (saturation at 65 535 ADU). The mean levels of the summed images and the variance in the difference of these images were determined. We have subtracted dark current from the flats and image statistics are performed within a section of  $120 \times 100$  square pixels, which is visually flat. A linear least-squares fitting of all the measurements gives:  $\sigma_{\text{ADU}}^2 = (54.10 \pm 0.03) + (0.843 \pm 0.008) \times \bar{S}$  ( $\sigma = 431.5 \text{ ADU}$ ), where  $\bar{S}$  refers to mean pixel counts. The transfer curve is formulated by

$$\sigma_{\text{ADU}}^2 = \frac{1}{g} \bar{S} + \frac{1}{g^2} \sigma_{\text{ron}}^2. \quad (\text{C.1})$$

The slope of this fitted line stands for the reciprocal gain. Thus, we graphically got the gain of  $1.186 \pm 0.011 e^-/\text{ADU}$ . From the fitted intercept we obtain read noise  $\sigma_{\text{ron}} = 8.7 \pm 0.2 e^-$  rms. The results are given in Figure C.4. As we actually work in the linear domain, a gain value of  $1.09 e^-$  rms which was indicated by the linearity trend drawn in the figure may be used. This figure also shows that the CCD is linear up to 35 000 ADU, about 53% of the saturation value. The factory's linear full well value of  $68\,000 e^-$  at medium gain of  $2 e^-/\text{ADU}$  (see Table 1) would correspond to 34 000 ADU, which confirms to our value. The deviation from linearity is distinctive when the counts are over 40 000. These measurements were acquired with the gain at low (hardware switch), but as stated in the previous section, the actual gain is controlled by both the CCD-controller and data-taking software and is working at the high gain setting.

We have also measured the gain and read noise with IRAF's *findgain* task. *Findgain* uses Janesick's method for determining the gain and read noise in a CCD from a pair of dome flat exposures and a pair of bias exposures (zero frames). We obtained two flats ( $F_1$  and  $F_2$ ) and two bias frames ( $B_1$  and  $B_2$ ). The calculations are given as follow:

$$\text{Gain} = \frac{(\overline{F_1} + \overline{F_2}) - (\overline{B_1} + \overline{B_2})}{\sigma_{(F_1-F_2)}^2 - \sigma_{(B_1-B_2)}^2}, \quad \text{Readnoise} = \frac{\text{Gain} \times \sigma_{(B_1-B_2)}}{\sqrt{2}} \quad (\text{C.2})$$

where the mean pixel values within each image are designated  $\overline{F_1}, \dots, \overline{B_2}$ , and the sum and difference images are expressed in formats as  $\overline{F_1} + \overline{F_2}$  and  $\overline{B_1} - \overline{B_2}$ . The tests give gain= $1.11 e^-/\text{ADU}$  and read noise of  $8.6 e^-$  rms. The results derived from the two approaches are consistent. At high and medium gains, the factory values are 1.00 and 1.98 for the 100-kHz readout speed, respectively, while for the

2-MHz speed they are 0.97 and 1.86, respectively. A twilight sky flat distribution at  $-45^\circ$  C and 100 kHz read rate along a central column and line is shown in Figure C.2.

#### Appendix D: *BVRI* THROUGHPUTS AND EXPOSURE GUIDE

To provide future observers with a helpful reference in estimating exposure times and signal-to-noise ratios for their targets, we have first intentionally measured the standard stars without bias, dark and flat corrections with MaxIm DL in order to obtain the maximum counts per pixel (the indicator for saturation and CCD linearity) and SNR for each standard star. These two parameters are most often a special concern for observers during observations of high-amplitude pulsating variables and eclipsing binaries. We used a uniform aperture radius, gap width and annulus thickness of 5, 6 and 6 pixels (matching seeing condition), respectively for all the stars' aperture photometry. In Table D.1, we list the results of ten standard stars which range from  $V = 10.5$  to 16.3 mag. Saturated values are given as 65535. The intensities ( $N_*$ , integration counts or electrons accumulated over the aperture) are not listed for all filters, but we list the mean count rates ( $\bar{n} \equiv N_*/n_{\text{pix}}$ , averaged counts per pixel) for *BV* filters and draw them (scaled as  $\log \bar{n}$ ) against the standard *BV* magnitudes in Figures D.1 and D.2 as a reference for throughput measurements. The linear fittings are given in Equations (D.1) and (D.2).

$$\log \bar{n}_B = 6.232 \pm 0.362 - (0.212 \pm 0.024) B, \quad \sigma = 0.154 \quad (\text{D.1})$$

$$\log \bar{n}_V = 6.892 \pm 0.157 - (0.262 \pm 0.011) V, \quad \sigma = 0.062 \quad (\text{D.2})$$

**Table D.1** Standard star throughput values acquired using *BVRI* filters at exposure times of 40, 20, 10 and 8 seconds, respectively. Below the magnitudes in each filter are the maximum counts in ADU and SNR. Mean count rates are only given for *BV* filters. A dash means no measurement.

Filter	Standard stars									
	98-185	98-670	98-666	98-676	98-682	98-966	98-581	98-627	98-L1	98-L4
B	10.742	13.286	12.894	14.216	14.382	14.469	14.798	15.589	16.913	17.674
	65535	11243	15469	4859	4185	3352	2700	1734	754	555
	—	1372	1917	528	489	368	325	172	—	26
$\bar{n}_B$	—	3387	4552	1559	1380	1260	1245	715	451	399
V	10.540	11.930	12.730	13.070	13.750	14.010	14.560	14.900	15.670	16.330
	65535	19539	10490	7095	4220	2823	2164	1676	884	613
	—	3019	1783	1071	561	304	269	228	—	56
$\bar{n}_V$	—	7040	4091	2746	1725	1478	1104	920	658	560
R	10.431	11.207	12.639	12.387	13.384	13.717	14.442	14.472	14.94	15.394
	48133	24405	7045	8249	3682	2255	1436	1427	951	653
	1395	3031	1102	792	—	304	172	190	—	71
I	10.309	10.555	12.530	11.718	13.033	13.387	14.199	14.083	14.225	14.604
	36275	28108	5197	9228	2957	1928	1178	1368	1223	937
	697	2718	635	675	—	199	123	155	—	85

Since we did not acquire these measurements at zenith but at an airmass of 1.32, we have attempted to correct the measured counts for extinction by using the extinction coefficients derived in the previous section. The linear fittings of the extinction corrected throughputs (see the dashed lines in Figures D.1 and D.2) would represent measurements at the zenith as

$$\log \bar{n}_{B,0} = 6.408 \pm 0.362 - (0.212 \pm 0.024) B, \quad \sigma = 0.154 \quad (\text{D.3})$$

$$\log \bar{n}_{V,0} = 7.008 \pm 0.157 - (0.262 \pm 0.011) V, \quad \sigma = 0.062 \quad (\text{D.4})$$

**Table D.2** Approximate Detection Limits at Different SNR and Exposure Times

SNR	$\Delta t$ (s)	<i>B</i>	<i>V</i>	<i>R</i>	<i>I</i>
200	1	11.3	11.6	11.7	11.4
100	1	12.7	13.0	13.1	12.9
200	3	12.5	12.8	12.9	12.6
100	3	13.9	14.2	14.3	14.0
200	5	13.0	13.3	13.4	13.1
200	10	13.8	14.1	14.1	13.8
200	20	14.5	14.8	14.8	14.5
200	30	14.9	15.2	15.2	14.9
200	60	15.6	15.9	15.9	15.5
200	90	16.0	16.2	16.2	15.8
200	180	16.6	16.8	16.6	16.3
100	180	17.7	17.9	17.7	17.3
200	300	17.0	17.3	17.1	16.7
100	300	18.1	18.2	18.1	17.6

Scaling with exposure time ( $\Delta t$ ), we can rewrite Equation (D.4) as  $\bar{n}_{v,0} = 509295 \Delta t \times 0.547^V$ . Adopting the ‘CCD equation’ (Howell 1989, PASP, 101, p.616)

$$\text{SNR} = \frac{N_*}{\sqrt{N_* + n_{\text{pix}}(N_s + N_d + N_r^2)}} \quad (\text{D.5})$$

and generally simplifying it to be

$$\text{SNR} \approx \sqrt{N_*} - \frac{1}{2} \frac{N_{(s,d,r)}}{\sqrt{N_*}} \quad (\text{D.6})$$

we may estimate SNR a bit easier. The individual terms are:  $N_*$ , the total number of photons (sky subtracted) from the star;  $n_{\text{pix}}$ , the number of pixels contained within the software aperture;  $N_s$ , the total number of sky photons per pixel;  $N_d$ , the dark current in photons per pixel; and  $N_r$ , the readout noise in electrons per pixel. For a bright star, usually  $N_{(s,d,r)} \ll \sqrt{N_*}$ ,  $\text{SNR} \approx \sqrt{N_*}$ . If total noise  $N_{(s,d,r)}$  is comparable with signal  $N_*$ , say half the value, then we can further get approximation  $\text{SNR} \approx 0.75\sqrt{N_*}$ . Assuming a photometry aperture of radius  $1.8 \times \text{FWHM} = 4.5$  pixels = 4.3 arcsec, corresponding to seeing of 2.5 arcsec, the common weather condition at the Xinglong station, at gain of  $1.17 \text{ e}^-/\text{ADU}$ , we have  $\sqrt{N_*} = 6156\sqrt{\Delta t \times 0.547^V}$ , thus we finally get

$$\text{SNR} \approx 4617\sqrt{\Delta t \times 0.547^V}. \quad (\text{D.7})$$

For instance, adopting the results given in Equation (D.7), for a star of  $V = 15$  mag with 20 seconds of exposure time, we might expect to obtain a mean count rate of  $1196 \text{ ADU pixel}^{-1}$  at zero airmass,  $\text{SNR} = 223$  and corresponding to a photometric accuracy of 0.0048 mag. The uncertainty in the star’s single magnitude is determined by

$$\sigma_{\text{mag}} = 2.5 \log\left(\frac{N_* + N_{(s,d,r)}}{N_*}\right) \approx 1.0857(N_{(s,d,r)}/N_*) = 1.0857/\text{SNR}. \quad (\text{D.8})$$

Please note that the actual observations highly depend on the weather conditions at the time, which may be a bit lower or higher than this expected value.

There is an easy way to estimate exposure time and SNR with IRAF’s CCDTIME task. Here we have edited two tables based upon the parameters corresponding to the present instrument system: (1) Moonless night sky brightness: 21.8, 20.9, 19.9, 18.9 mag arcsec<sup>-2</sup> (Liu Y. et al. 2003, PASP, 115, p.495); detective quantum efficiency 0.53, 0.68, 0.73, 0.80 and extinction coefficients of 0.33, 0.24,

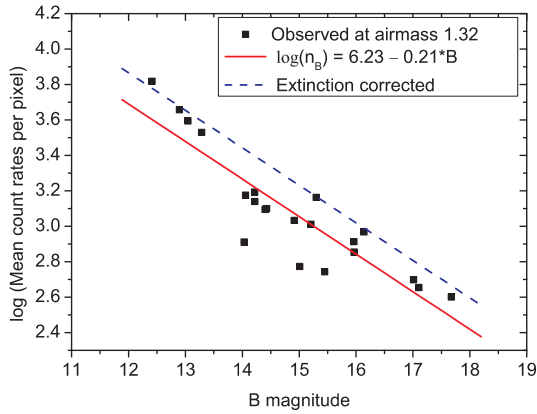


**Fig. D.1** Throughput values of standard stars acquired using the *B* filter at exposure time 40 seconds.

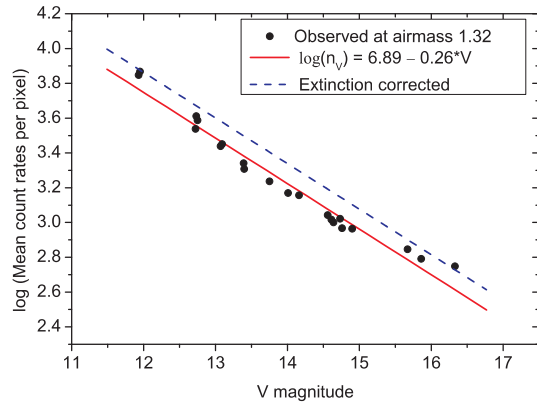


**Fig. D.2** Throughput values of standard stars acquired using the *V* filter at exposure time 20 seconds.

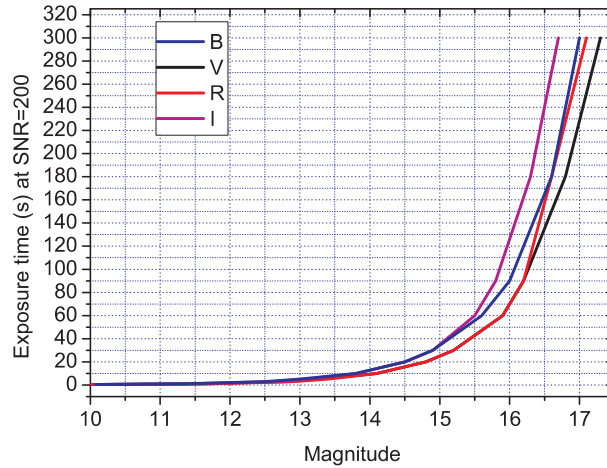


**Fig. D.3** Approximate exposure times at SNR=200 as a function of magnitudes.

**Table D.3** Approximate Exposure Guide at SNR=200 Times in Seconds

SNR	mag	<i>B</i>	<i>V</i>	<i>R</i>	<i>I</i>
200	17	792.18	285.40	218.62	246.90
200	16	91.69	69.16	70.72	115.42
200	15	33.04	24.71	23.80	34.12
200	14	12.61	9.39	8.79	11.71
200	13	4.93	3.67	3.39	4.37
200	12	1.95	1.45	1.33	1.69
200	11	0.77	0.58	0.53	0.67
200	10	0.31	0.23	0.21	0.26

## Differential light curves

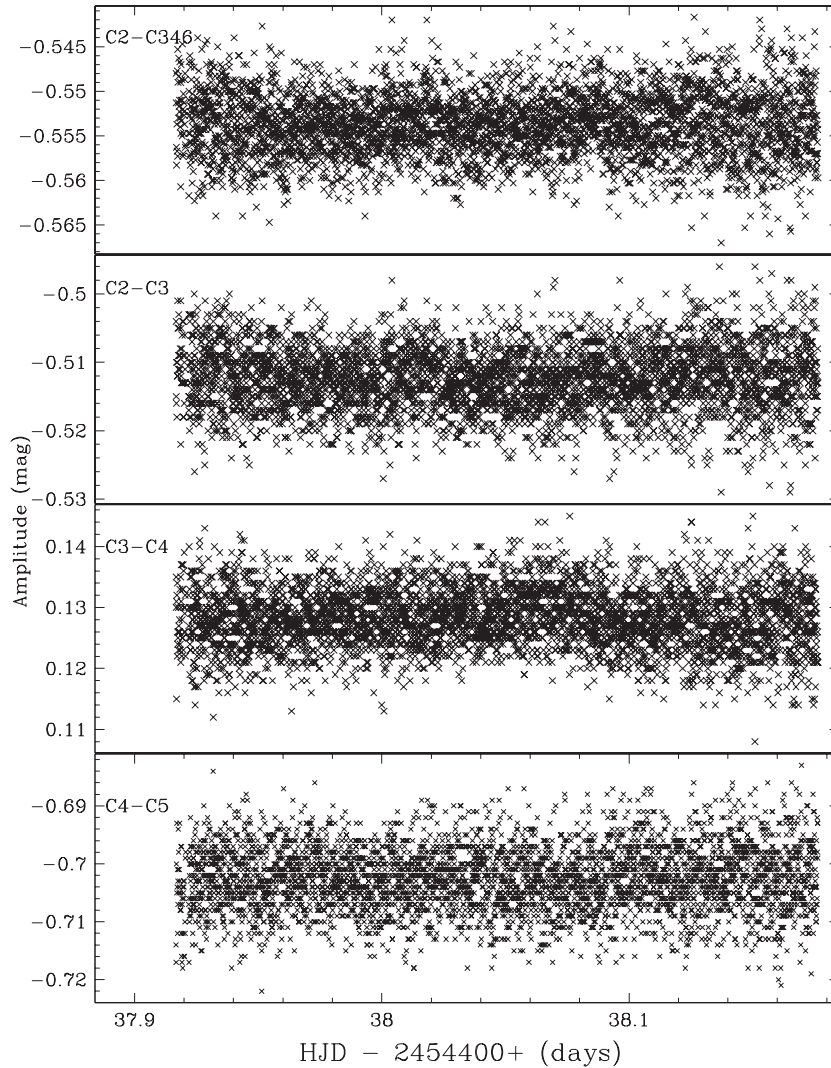


**Fig. D.4** Four sets of differential light curves ( $V$  filter) among five field stars around V577 Oph. ‘C2–C346’ stands for  $C2-(C3+C4+C6)/3$ .

0.19, 0.07 magnitudes per airmass for  $BVRI$ , respectively. (2) read noise  $8 e^-$ , dark rate  $7.8 e^-/s$ , pixel size  $13 \mu m$ . (3) seeing 2.5 arcsec, unbinned, at zero airmass and zero Moon phase. We can see for stars of  $V = 15$  mag, the results in Tables D.2 and D.3 could predict an exposure time of 25 seconds with  $SNR=200$ , which is consistent with that estimated above. Within 5 minutes of exposure, one may observe stars of  $V = 18.2$  mag with  $SNR=100$  or  $V = 17.3$  mag with  $SNR=200$ ; this could act as a detection limit for a time-resolution demanded photometer on the 85-cm telescope. We plot a complex exposure guide for the  $BVRI$  filters in Figure D.3. Caution must be taken when referring to these tables and figures because they are estimated under the above condition of ideal parameters.

However, we must be aware that the SNR values given by MaxIm DL are over-estimated and are higher than the approximation,  $\sqrt{N_*}$ , which is simplified for the case of stars much brighter than background, while they are under-estimated for fainter stars. This is why we calculate SNR for each frame online as described in Equation (D.5). The online SNR is actually indicative of photometric accuracy. By comparison we found that the MaxIm DL's SNR usually must be higher than 100.

## References

- Bessell, M. S. 1990, *PASP*, 102, 1181  
Cousins, A. W. J., & Caldwell, J. A. R. 2001, *MNRAS*, 323, 380  
Landolt, A. U. 1992, *AJ*, 104, 340  
Shi, H.-M., et al. 1998, *AcApS*, 18, 99  
Walker, A. R. 1990, In G. H. Jacoby, ed., *ASP Conf. Ser.*, Vol.9, *CCDs in Astronomy* (San Francisco: ASP), 319  
Zhou, A.-Y., An, D., Eggen, J. R., Reed, M. D., Terndrup, D. M., & Harms, S. L. 2006, *Ap&SS*, 305, 29